

GATS: Gaussian Aware Temporal Scaling Transformer for Invariant 4D Spatio-Temporal Point Cloud Representation

Jiayi Tian

State Key Laboratory of Human-Machine Hybrid Augmented Intelligence
Institute of Artificial Intelligence and Robotics, Xi'an Jiaotong University

tianreg@stu.xjtu.edu.cn

Jiaze Wang

Harbin Institute of Technology, Shenzhen, Pengcheng Laboratory

24b951071@stu.hit.edu.cn

Abstract

*Understanding 4D point cloud videos is essential for enabling intelligent agents to perceive dynamic environments. However, temporal scale bias across varying frame rates and distributional uncertainty in irregular point clouds make it highly challenging to design a unified and robust 4D backbone. Existing CNN or Transformer based methods are constrained either by limited receptive fields or by quadratic computational complexity, while neglecting these implicit distortions. To address this problem, we propose a novel dual invariant framework, termed **Gaussian Aware Temporal Scaling (GATS)**, which explicitly resolves both distributional inconsistencies and temporal. The proposed Uncertainty Guided Gaussian Convolution (UGGC) incorporates local Gaussian statistics and uncertainty aware gating into point convolution, thereby achieving robust neighborhood aggregation under density variation, noise, and occlusion. In parallel, the Temporal Scaling Attention (TSA) introduces a learnable scaling factor to normalize temporal distances, ensuring frame partition invariance and consistent velocity estimation across different frame rates. These two modules are complementary: temporal scaling normalizes time intervals prior to Gaussian estimation, while Gaussian modeling enhances robustness to irregular distributions. Our experiments on mainstream benchmarks MSR-Action3D (+6.62% accuracy), NTU RGBD (+1.4% accuracy), and Synthia4D (+1.8% mIoU) demonstrate significant performance gains, offering a more efficient and principled paradigm for invariant 4D point cloud video understanding with superior accuracy, robustness, and scalability compared to Transformer based counterparts.*

1. Introduction

4D point cloud videos, which extend 3D space with 1D time, provide a natural representation of dynamic physical environments by capturing both geometric structures and temporal motions [48]. They are increasingly important for enabling intelligent agents to perceive dynamics, understand environmental changes, and interact effectively with the world [57]. Consequently, point cloud video modeling has attracted growing attention [11, 34, 51], with applications spanning robotic [35], AR/VR [42], and SLAM systems [4, 31].

Despite the remarkable progress in static 3D point cloud understanding [11, 35, 51], building effective backbones for dynamic 4D point cloud sequences remains a significant challenge [24]. Unlike conventional RGB videos with structured grids [21], point cloud videos are inherently irregular and unordered in space, making grid based methods such as 3D convolutions [45] unsuitable. A straightforward approach is voxelization [50], which converts raw 4D sequences into structured grids for 4D convolutions. However, voxelization inevitably introduces quantization errors [26] and suffers from inefficiency due to the sparsity and scale of 4D data [57]. Another line of research [9, 10, 58] directly processes raw 4D sequences using convolutional networks [27] or transformers [5, 38]. Yet, CNNs are limited by their local receptive fields [33], while transformers incur quadratic complexity [45].

Beyond efficiency and scalability, we identify two fundamental distortions in point cloud video modeling—complementary facets of a unified spatio-temporal misrepresentation (Fig. 1): (1) **Distributional uncertainty**: current geometric convolutions only consider Euclidean distances, ignoring local distributional shape and uncertainty. Dynamic point clouds, however, naturally exhibit

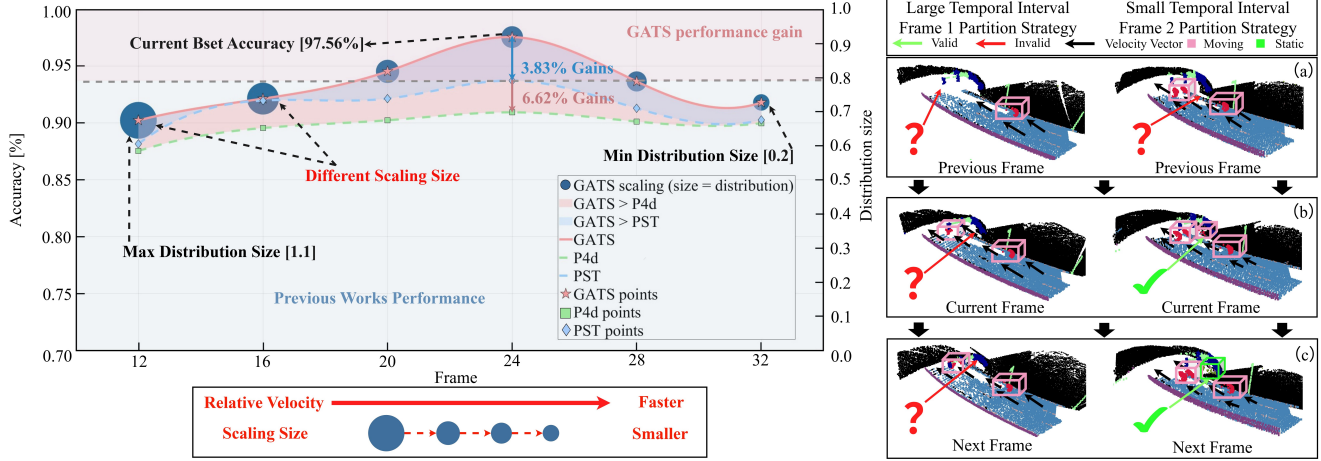


Figure 1. Motivation. **Right:** The right panel illustrates video sequences under different frame rate partitions: with a large temporal interval, some moving objects (second row) and static objects (third row) disappear, while they remain visible with a small temporal interval. This indicates that varying frame rate partitions may cause certain velocity features to vanish. **Left:** The left panel illustrates that GATS can adaptively adjust the scaling distribution across different frame rate partitions, thereby effectively mitigating the relative velocity bias introduced by frame rate variations and reducing fluctuations in accuracy. Consequently, GATS achieves improvements in ACC of 6.62% and 3.83% over P4D and PST, respectively.

density variation, noise, occlusion, and missing points, which degrade robustness. (2) **Temporal scale bias:** Under different frame intervals, the same physical motion may be discretized into different relative velocity estimates, leading to inconsistencies and distortions in spatio-temporal representations. Existing methods typically rely on fixed frame partitioning or sampling rates.

Motivated by these observations, we propose **Gaussian Aware Temporal Scaling (GATS)**, a dual-invariant Transformer framework for 4D point cloud video modeling. The central insight is that a collaborative calibration mechanism is required to jointly normalize geometric distributions and temporal motions, thereby achieving truly invariant and robust spatio-temporal representations. Specifically, we introduce two complementary modules: (1) **Uncertainty Guided Gaussian Convolution (UGGC)** that augments geometric kernels with Gaussian statistics (mean, covariance, and uncertainty indicators), enabling robust neighborhood aggregation under density variation and noise. different frame rates. (2) **Temporal Scaling Attention (TSA):** with a learnable normalization factor, it enables velocity-invariant temporal modeling, ensures consistent frame partitioning, and reduces distortions across frame rates.

These two modules are naturally synergistic: temporal scaling normalizes time intervals before Gaussian estimation, preventing variance inflation across different frame rates, while Gaussian modeling provides distributional robustness for spatio-temporal neighborhoods. The pipeline is shown in Fig. 2. To the best of our knowledge, this is the **first work** to explicitly introduce relative velocity estimation in spatio-temporal point cloud modeling.

Overall, our main contributions are as follows:

- We propose a novel 4D backbone, **GATS**, that explicitly addresses two implicit distortions in point cloud video modeling: temporal scale bias and distributional uncertainty.
- We introduce an **UGGC module** that incorporates local Gaussian statistics and uncertainty aware gating into P4DConv, enhancing robustness to noise, occlusion, and density variation.
- We design a **TSA module** that achieves frame partition invariance by rescaling temporal metrics, improving consistency across varying frame rates and sampling strategies.
- Extensive experiments on multiple 4D understanding benchmarks demonstrate that GATS achieves superior performance and robustness compared to baseline methods, while maintaining high efficiency and scalability.

2. Related Work

2.1. Backbones for 4D point cloud videos: CNNs, Transformers, and SSMs

Backbones for dynamic 4D point cloud sequences have evolved along three major paradigms: CNNs, Transformers, and State Space Models (SSMs) [4, 5, 18]. Early CNN based methods either convert raw 4D sequences into structured grids (*e.g.*, voxels or BEV) to apply 3D/4D convolutions, or directly operate on raw points with spatio-temporal kernels [6]. While grid conversion enables standard convolutions, it introduces quantization artifacts and loses geometric fidelity; point based CNNs are constrained by lo-

cally restrained receptive fields and limited long range temporal modeling. Transformer based backbones [5] enlarge receptive fields using global self-attention and often pair local point convolutions with temporal attention across timestamps; efficiency oriented variants employ compact mid-level tokens or self-supervised training to mitigate annotation cost. However, quadratic complexity and sensitivity to frame partitioning remain bottlenecks, leading to high overhead and temporal scale bias under varying sampling strategies. Recently, SSM based designs (e.g., Mamba style modules [28, 53]) achieve linear complexity for long sequence modeling via parallel scans and data dependent state transitions, offering scalable temporal coverage with global receptive fields. Distinct from prior art, our framework emphasizes *dual invariance*: it mitigates temporal scale bias through temporal scaling attention and enhances distributional robustness via Gaussian aware convolution, complementing architectural efficiency with invariance aware modeling.

2.2. Geometric modeling on dynamic 4D point clouds

Research on geometric modeling for dynamic point clouds follows two threads: (i) *dynamic as signal* methods that take temporal variation itself as the modeling target [23, 32], and (ii) *geometry only* methods that rely on static descriptors without explicit temporal reasoning [13]. Dynamic as signal approaches explicitly track points or estimate scene flow to align correspondences across frames, enabling motion aware grouping and temporal aggregation (e.g., recurrent point modules and PointNet++ extensions with temporal grouping or flow based alignment [33, 34]). While explicit motion preserves identities, performance is sensitive to tracking errors, motion inconsistency, and point entry/exit in sparse or noisy scenes. Subsequent methods (e.g., PST style spatio temporal convolutions [4, 5, 18]) construct 4D neighborhoods to learn motion patterns implicitly without hard associations, improving robustness but remaining limited by local receptive fields. Geometry only approaches emphasize robust per frame spatial descriptors and aggregate them across time, avoiding explicit tracking or flow. Typical designs use Euclidean kernels, anisotropic neighborhood selection, and hierarchical local feature extraction [12]; hybrid voxel–point pipelines alleviate sparsity and efficiency issues but still lack explicit statistical modeling. To address these limitations, distribution aware schemes introduce statistical cues (e.g., Gaussian weighting, covariance guided anisotropy) into neighborhood aggregation. Our method advances this direction with *multi-scale Gaussian weighting* for heterogeneous densities and *uncertainty aware gating* via covariance conditioning, yielding distributionally robust features without explicit tracking.

2.3. Spatio-temporal decoupled representations for 4D point cloud videos

Decoupling space and time is a pragmatic strategy for 4D point clouds: spatial sampling is irregular and unordered, whereas temporal sampling is typically regular [8]. Prior frameworks commonly adopt a two branch design that combines *intra frame spatial encoding* for local geometric patterns with *inter frame temporal modeling* for long range dependencies. Intra frame modules include point based CNNs and local operators (e.g., PointNet++ variants and PST style kernels [5, 33, 37]) that build robust neighborhoods, perform hierarchical aggregation, and leverage anisotropic receptive fields; hybrid voxel–point tokens provide compact intermediate representations but introduce quantization artifacts. Inter frame modules range from RNNs and temporal pooling to global attention and SSMs: Transformers (e.g., temporal attention over all timestamps [18, 22]) capture global semantics at quadratic cost, while Mamba style SSMs provide linear time long sequence coverage via data dependent state transitions and parallel scans. Despite the effectiveness of decoupling, most methods assume fixed frame rates or uniform partitions, which induces (1) *temporal scale bias*: identical physical motion maps to different discrete temporal distances and velocities under varying sampling. Moreover, spatial neighborhoods are commonly treated with purely geometric kernels, overlooking (2) *distributional uncertainty* (density variation, anisotropy, noise, and missing points).

We retain the decoupling principle and introduce two invariance oriented components: (1) *UGGC module*, which encodes local shape statistics (mean and covariance) together with uncertainty within spatial neighborhoods; (2) *TSA module*, which normalizes temporal metrics and ensures frame partition invariance. This design mitigates temporal scale bias, promotes consistent representations across varying frame rates, and enhances the stability of spatio-temporal modeling. Together, these modules yield decoupled features that remain consistent across frame rates and robust to heterogeneous local distributions, while integrating seamlessly with CNN, Transformer, and SSM backbones.

3. Methodology

3.1. Problem Definition

We consider a point cloud video sequence \mathcal{P} as follows:

$$\mathcal{P} = \{P_t\}_{t=1}^T, \quad P_t = \{(x_i^t, T f_i^t)\}_{i=1}^{N_t}, \quad (1)$$

where P_t is the point clouds of each video frame, $x_i^t \in \mathbb{R}^3$ denotes the 3D coordinate of the i -th point at frame t , $T f_i^t \in \mathbb{R}^d$ indicates the associated temporal feature, and N_t is the number of points in frame t . The goal is to learn a

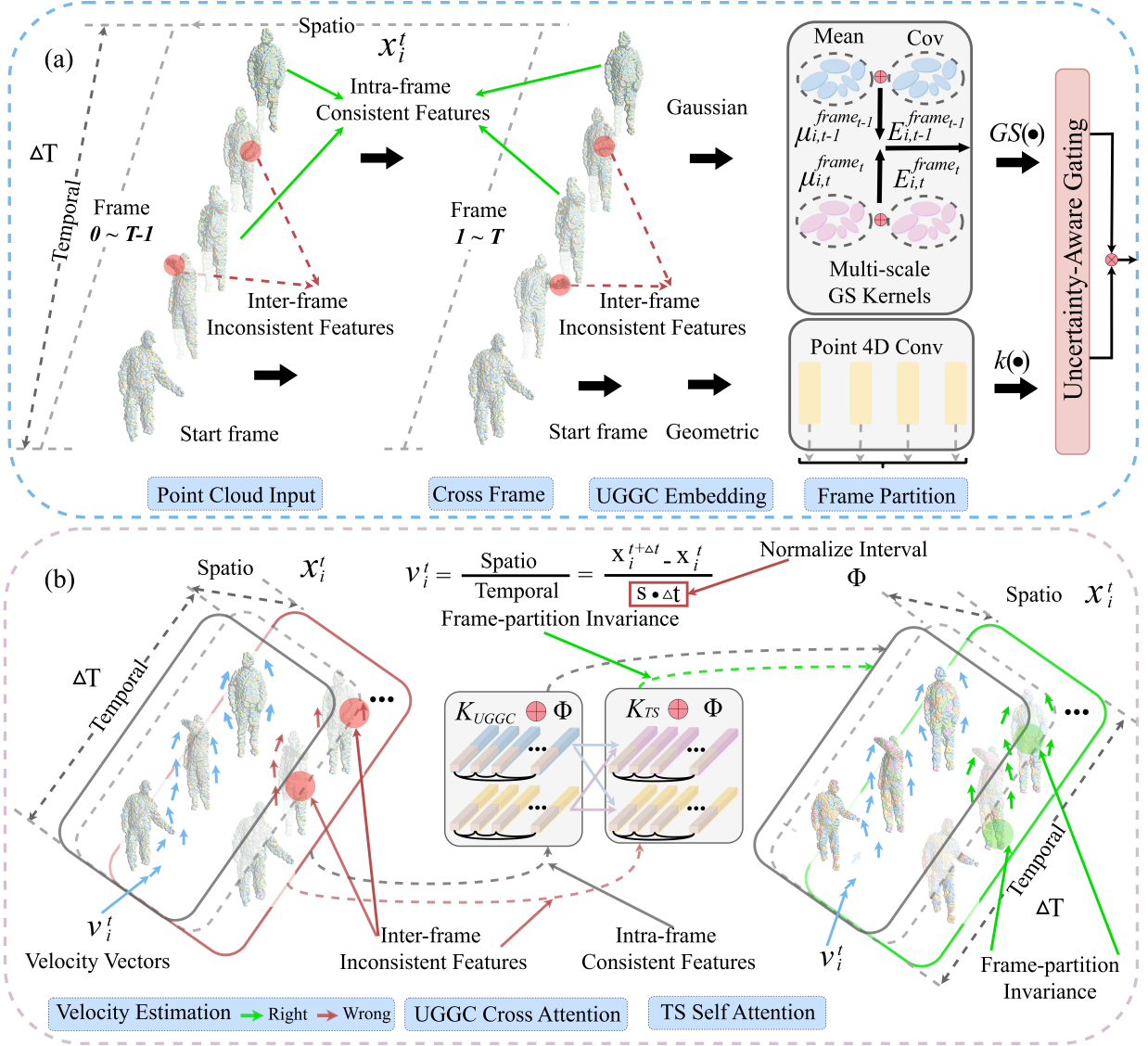


Figure 2. Pipeline. The overall network backbone consists of two core modules: **(a) UGGC Module**. After the point cloud is fed into the network, the spatial variations of x_i^t generate cross frame representations. However, different cross frames often lead to inter frame inconsistencies. The UGGC module extracts local Gaussian features and incorporates an uncertainty aware gating mechanism to jointly model geometric and Gaussian local features of 4D point clouds, thereby enhancing the robustness of feature extraction. **(b) TSA Module**. Under different frame rates, the estimation of relative velocity v_i^t varies, and as the temporal dimension progresses, motion features tend to produce inter frame inconsistencies. To address this, the TSA module introduces a learnable scaling factor s to normalize temporal distances, achieving frame partition invariance and ensuring consistent relative velocity estimation across varying frame rates.

spatio-temporal modeling function \mathcal{F} that maps $\{P_t\}_{t=1}^T$ to a target output y .

$$\mathcal{F} : \{P_t\}_{t=1}^T \mapsto y, \quad (2)$$

where y can be an action label, per point segmentation mask, or video modeling.

Compared with conventional videos, point cloud videos face two key distortions: (i) **Distributional uncertainty** from irregular geometry and noise. (ii) **Temporal scale bias**

from inconsistent relative velocity estimates under varying frame rates.

Moreover, uncalibrated geometric representations distort motion perception, while unnormalized motion interferes with geometric understanding. This dual dilemma must be resolved through a complementary fusion framework. To address these issues, we propose **Gaussian Aware Temporal Scaling (GATS)**, a dual-invariant framework that introduces (2) *Uncertainty Guided Gaussian Convolution* for

distributional robustness, and (2) *Temporal Scaling Attention* for frame partition invariance.

3.2. Uncertainty Guided Gaussian Convolution

Geometric convolutions typically rely on Euclidean distance, ignoring local distributional shape and uncertainty. Dynamic point clouds, however, exhibit density variation, noise, and occlusion. We propose to incorporate Gaussian statistics into 4D Points convolution to enhance robustness.

Local Gaussian Estimation. For a center point x_i^t , its 4D neighborhood $N(i, t)$ is modeled by mean and covariance:

$$\mu_{i,t} = \frac{1}{|N(i, t)|} \sum_{x_i^t \in N(i, t)} x_i^t, \quad (3)$$

$$\Sigma_{i,t} = \frac{1}{|N(i, t)|} \sum_{x_i^t \in N(i, t)} (x_i^t - \mu_{i,t})(x_i^t - \mu_{i,t})^\top. \quad (4)$$

Here $\mu_{i,t} \in \mathbb{R}^3$ is the local centroid, and $\Sigma_{i,t} \in \mathbb{R}^{3 \times 3}$ encodes distributional anisotropy.

Gaussian Weighted Convolution. Building upon this estimation, we design a Gaussian weighted convolution that integrates both geometric kernels $k(\cdot)$ and Gaussian statistical $GS(\cdot)$ likelihoods. The aggregation weight is defined as:

$$w(x) = k(x_i^t - \mu_{i,t}) \cdot \exp\left(-\frac{1}{2}(x_i^t - \mu_{i,t})^\top \Sigma_{i,t}^{-1} (x_i^t - \mu_{i,t})\right). \quad (5)$$

To further adapt to heterogeneous densities, we employ multi-scale Gaussian kernels with $\sigma \in \{0.5r, r, 3r\}$.

Uncertainty Aware Gating. While Gaussian weighting improves robustness, the reliability of local statistics may still vary under severe noise or occlusion. To adaptively balance standard and robust features, we introduce an uncertainty aware gating mechanism. Using the condition number $\text{cond}(\Sigma_{i,t})$ or its eigenvalue spectrum as an uncertainty indicator, we define:

$$f' = \alpha f + (1 - \alpha) f_{\text{robust}}, \quad \alpha = \phi(\text{cond}(\Sigma_{i,t})), \quad (6)$$

where f is the standard convolution feature, f_{robust} is a complementary branch (e.g., larger receptive field), and $\phi(\cdot)$ maps uncertainty to $[0, 1]$. This gating ensures that the model adaptively emphasizes robust features when uncertainty is high, while preserving efficiency in stable regions.

3.3. Temporal Scaling Attention

Existing Transformer based models often rely on discrete frame indices $|t - t'|$ as temporal bias. However, the same physical motion may correspond to different discrete intervals Δt under varying frame rates, leading to inconsistent velocity estimation. To address this temporal scale bias, we

introduce a temporal scaling factor that normalizes such discrepancies and ensures consistent motion representation.

Relative Velocity. First, given a point $x_i^t \in \mathbb{R}^3$ at time t , the relative velocity $v_i^t \in V_i^t$ is defined as:

$$v_i^t = \frac{x_i^{t+\Delta t} - x_i^t}{\Delta t}, \quad (7)$$

where $\Delta t \in \Delta T$ denotes the frame interval. To eliminate the dependency on arbitrary frame rates, we introduce a learnable or estimable scaling factor $s \in \mathbb{R}^+$:

$$\Delta t' = s \cdot \Delta t, \quad v_i^t = \frac{x_i^{t+\Delta t} - x_i^t}{s \cdot \Delta t}. \quad (8)$$

This normalization ensures that velocity estimation remains consistent across different temporal partitions.

Temporal Scaling Attention. Building upon this formulation, we embed the scaling factor into the attention mechanism. Specifically, the scaled temporal distance modifies the positional bias:

$$\text{Attn}(q_t, k_{t'}) = \frac{q_t k_{t'}^\top}{\sqrt{d}} + \beta \cdot \Phi(s \cdot |t - t'|), \quad (9)$$

where $q_t, k_{t'} \in \mathbb{R}^d$ are query and key vectors. In our design, the key vector further integrates two complementary components: K_{UGGC} from the Uncertainty Guided Gaussian Convolution branch and K_{TS} from the Temporal Scaling branch; $\Phi(\cdot)$ maps temporal distance to bias, and β is a learnable weight. Unlike conventional additive bias, this scaling redefines the temporal metric space, thereby achieving frame partition invariance.

Geometric Feature Extraction. The temporal scaling factor also benefits geometric feature extraction. In P4D convolution, the temporal neighborhood radius r_t is rescaled as:

$$r_t' = s \cdot r_t, \quad (10)$$

which guarantees consistent neighborhood selection regardless of frame rate variations.

Synergy with Temporal Scaling. Finally, temporal scaling naturally complements Gaussian based modeling. By normalizing the temporal radius after Gaussian estimation, it prevents variance inflation across different frame rates and ensures the comparability of Gaussian attributes. This synergy highlights the dual role of temporal scaling: stabilizing motion representation and enhancing distributional robustness.

4. Experiments

4.1. Experimental Setup

Our experimental validation is performed on three widely recognized benchmarks. For the 3D action recognition

Table 1. Action recognition accuracy comparison (%) on MSR-Action3D.

Methods	Input	Frames	Accuracy (%)
Actionlet [44]	skeleton	all	88.21
MeteorNet [25]	point	12	86.53
PSTNet [6]	point	12	87.88
P4Transformer [5]	point	12	87.54
PST-Transformer [8]	point	12	88.15
GATS (Ours)	point	12	90.24
Vieira et al. [43]	depth	20	78.20
GATS (Ours)	point	20	94.54
MeteorNet [25]	point	24	88.50
PSTNet [6]	point	24	91.20
P4Transformer [5]	point	24	90.94
PST-Transformer [8]	point	24	93.73
PSTNet++[7]	point	24	92.68
PPTr+C2P[56]	point	24	94.76
PointCPSC[38]	point	24	92.68
MaST-Pre[37]	point	24	94.08
SequentialPointNet[17]	point	24	92.64
MAMBA4D[22]	point	24	93.38
3DInAction[1]	skeleton	24	92.23
PvNeXt[46]	point	24	94.77
GATS (Ours)	point	24	97.56

task, we utilize MSR-Action3D [16] and NTU RGBD [36]. For 4D semantic segmentation, we employ the Synthia 4D dataset [3]. A comprehensive description of the experimental dataset can be found in Appendix 1.1. Additionally, further details regarding the experimental settings are presented in Appendix 1.2.

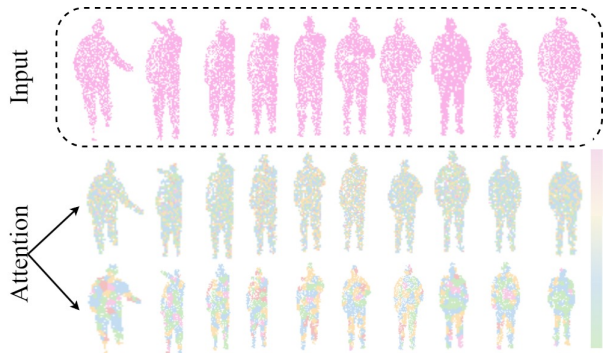


Figure 3. MSR-attention Results. Attention visualization showing focus on key regions and spatio-temporal dynamics.

4.2. MSR-Action3D

Quantitative results. Table 1 reports the performance of GATS on the MSR-Action3D benchmark. In the 24-frame setting, GATS achieves the highest accuracy of 97.56%, outperforming the lowest-performing recent model MAMBA4D (93.38%) by over 4 points. Compared

Table 2. Action recognition accuracy (%) on NTU RGBD.

Method	Input	Acc (%)
SkeleMotion[2]	skeleton	69.6
GCA-LSTM[20]	skeleton	74.4
AttentionLSTM[19]	skeleton	77.1
AGC-LSTM[41]	skeleton	89.2
AS-GCN[15]	skeleton	86.8
VA-fusion[55]	skeleton	89.4
2s-AGCN[40]	skeleton	88.5
DGNN[39]	skeleton	89.9
HON4D[30]	depth	30.6
SNV[54]	depth	31.8
HOG ² [29]	depth	32.2
Li et al.[14]	depth	68.1
Wang et al.[47]	depth	87.1
MVDI[52]	depth	84.6
PointNet++[33]	point	80.1
3DV[49]	voxel	84.5
3DV-PointNet++[49]	voxel+point	88.8
PSTNet[6]	point	90.5
P4Transformer[5]	point	90.2
PST-Transformer[8]	point	91.0
SequentialPointNet[17]	point	90.3
MaST-Pre[37]	point	90.8
PvNeXt[46]	point	89.2
GATS(Ours)	point	91.7

with strong baselines such as PvNeXt (94.77%) and PST-Transformer (93.73%), GATS also shows clear improvements. Consistent gains are observed in other settings, reaching 94.54% at 20 frames and 90.24% at 12 frames.

Qualitative results. We further visualize attention weights in Fig. 3. The results show that the Transformer focuses on relevant regions across frames and highlights key transitional parts of actions. This confirms that our attention mechanism effectively captures spatio-temporal dynamics and can serve as a substitute for explicit point tracking.

4.3. NTU RGBD

Quantitative results. The evaluation of action recognition accuracy on the NTU RGB+D dataset is detailed in Tab. 2. Our model, which operates directly on point cloud inputs, achieves a new state-of-the-art accuracy of 91.7%. This performance surpasses all other listed methods, including strong point based competitors like PST-Transformer (91.0%) and MaST-Pre (90.8%). Furthermore, our model outperforms the hybrid voxel+point method, 3DV-PointNet++ (88.8%), by a significant margin of 2.9%. This result highlights our framework’s superior ability to capture complex spatio-temporal dynamics from raw

Table 3. 4D semantic segmentation results (mIoU %) on the Synthia 4D dataset.

Method	Input	Frame	Track	Bldn	Road	Sdwlk	Fence	Vegittn	Pole	-
3D MinkNet14	voxel	1	-	89.39	97.68	69.43	86.52	98.11	97.26	-
4D MinkNet14	voxel	3	-	90.13	98.26	73.47	87.19	99.10	97.50	-
PointNet++	point	1	-	96.88	97.72	86.20	92.75	97.12	97.09	-
MeteorNet-m	point	2	✓	98.22	97.79	90.98	93.18	98.31	97.45	-
MeteorNet-m	point	2	×	97.65	97.83	90.03	94.06	97.41	97.79	-
MeteorNet-l	point	3	×	98.10	97.72	88.65	94.00	97.98	97.65	-
P4Transformer	point	1	-	96.76	98.23	92.11	95.23	98.62	97.77	-
P4Transformer	point	3	×	96.73	98.35	94.03	95.23	98.28	98.01	-
PST-Transformer	point	1	-	94.46	98.13	89.37	95.84	99.06	98.10	-
PST-Transformer	point	3	×	96.10	98.44	94.94	96.58	98.98	98.10	-
MAMBA4D	point	3	×	96.16	98.58	92.80	94.95	97.08	98.24	-
GATS(Ours)	point	1	×	97.51	98.58	95.62	95.54	99.01	98.27	-
GATS(Ours)	point	3	×	97.37	98.41	94.72	95.85	97.81	98.31	-

Method	Input	Frame	Track	Car	T. Sign	Pedstrn	Bicycl	Lane	T. Light	mIoU
3D MinkNet14	voxel	1	-	93.50	79.45	92.27	0.00	44.61	66.69	76.24
4D MinkNet14	voxel	3	-	94.01	79.04	92.62	0.00	50.01	68.14	77.46
PointNet++	point	1	-	90.85	66.87	78.64	0.00	72.93	75.17	79.35
MeteorNet-m	point	2	✓	94.30	76.35	81.05	0.00	74.09	75.92	81.47
MeteorNet-m	point	2	×	94.15	82.01	79.14	0.00	72.59	77.92	81.72
MeteorNet-l	point	3	×	93.83	84.07	80.90	0.00	71.14	77.60	81.80
P4Transformer	point	1	-	95.46	80.75	85.48	0.00	74.28	74.22	82.41
P4Transformer	point	3	×	95.60	81.54	85.18	0.00	75.95	79.07	83.16
PST-Transformer	point	1	-	96.80	80.41	87.58	0.00	75.25	80.84	82.92
PST-Transformer	point	3	×	96.06	82.67	87.86	0.00	76.01	81.67	83.95
MAMBA4D	point	3	×	95.75	82.03	84.57	0.00	79.35	80.74	83.35
GATS(Ours)	point	1	×	95.62	81.08	83.11	0.00	77.19	83.12	83.72
GATS(Ours)	point	3	×	95.80	84.87	87.64	0.00	76.77	82.98	84.21

point sequences, establishing its effectiveness for 3D action recognition.

4.4. 4D Semantic Segmentation

Quantitative results. As delineated in Tab. 3, our model’s 4D semantic segmentation performance was comprehensively benchmarked against state-of-the-art methods on the Synthia 4D dataset. In the challenging multi-frame (frame=3) setting, our model achieves a new state-of-the-art mIoU of 84.21%, surpassing the previous best, PST-Transformer. Our model also establishes its superiority in the single frame (frame=1) setting, attaining an mIoU of 83.72% and outperforming all competitors. The significant performance gain from the single frame to the multi frame variant (83.72% to 84.21%) effectively demonstrates our ar-

chitecture’s robust ability to leverage temporal information, firmly establishing its overall superiority.

Qualitative results. Figure 4 presents a qualitative analysis, comparing our model’s predictions against the raw input and GT segmentation. The visualizations confirm that our predictions align closely with the GT across varied and complex scenes. This ability to accurately capture intricate boundaries and fine-grained details underscores the model’s high fidelity and strong generalization.

4.5. Ablation Studies

To validate the contribution of each key component, we conducted ablation studies on the MSR-Action3D dataset, with results detailed in Tab. 4. The full model serves as our baseline, achieving an accuracy of 97.56%. When the GA mod-

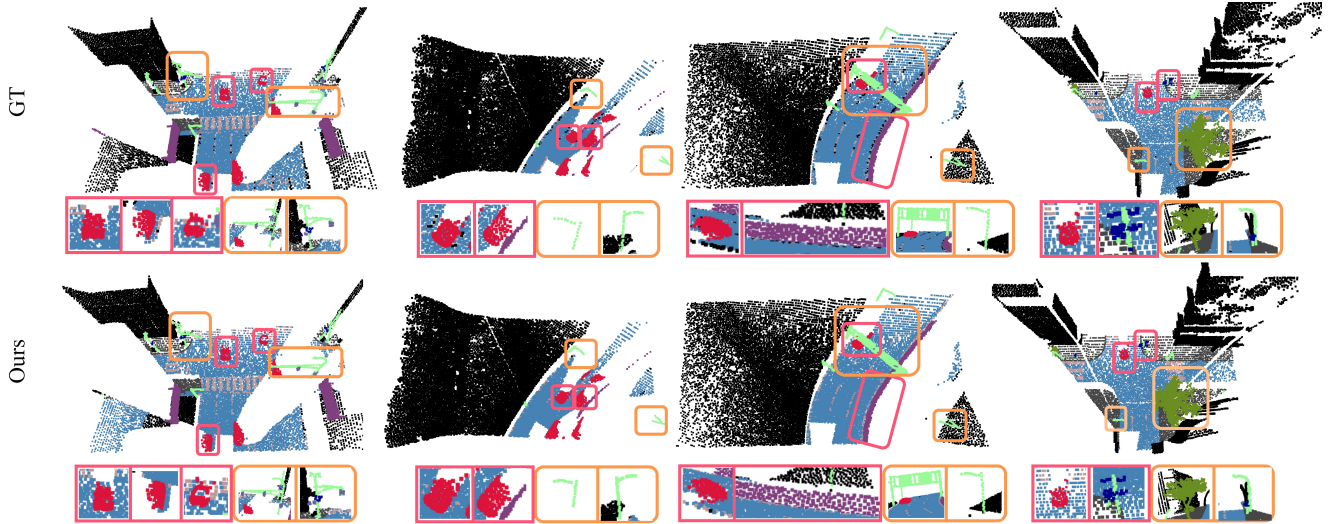


Figure 4. 4D Qualitative Results. The rows from top to bottom correspond to the input, GT, and our predictions. Detailed comparative results are highlighted in the enlarged regions of the figure.

ule was removed (“w/o GA”), the accuracy experienced a notable drop to 95.12%. Similarly, excluding the TS module (“w/o TS”) reduced the accuracy to 96.16%. This clear performance degradation upon the removal of either component confirms that both GA and TS are integral to the model’s success.

Table 4. Ablation studies on MSR-Action3D.

Model	frame	Acc(%)
(a) Full Model	24	97.56
(b) w/o UGGC	24	95.12
(c) w/o TSA	24	96.16
(d) PSTTransformer (baseline)	24	93.73

Table 5. Comparison results with advanced architecture processing more frames.

Method	Backbone	Frame	Acc(%)
PvNeXt	CNN	24	94.77
MAMBA4D	Mamba	24	93.38
Ours	Transformer	24	97.56

Comparative Study on Model Effectiveness and Efficiency. In our comparative analysis (Tab. 5), the Transformer model achieved 97.56% accuracy with 24 frames, outperforming MAMBA4D (32 frames, 93.38%) and PvNeXt (24 frames, 94.77%). This result demonstrates not only superior spatio-temporal modeling capability but also greater efficiency. In contrast to models that

rely on more frames but yield lower accuracy, our approach achieves superior performance and thus provides a more practical solution for long-sequence tasks.

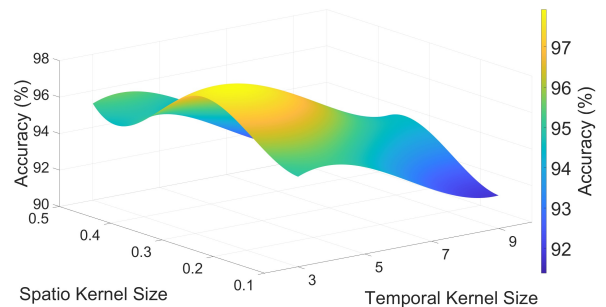


Figure 5. Analysis of accuracy with varying temporal and spatial parameters.

Effect of temporal kernel size and spatial radius. Figure 5 illustrates the ablation study on temporal kernel size and spatial radius. The analysis reveals that smaller temporal kernels are advantageous, as the model achieves its peak accuracy at the smallest tested size of 3, after which performance monotonically decreases with larger kernels. In contrast, the spatial radius requires an optimal balance; accuracy improves from a radius of 0.1, peaks at 97.56% with a radius of 0.3, and then distinctly degrades at larger values.

5. Conclusion

We propose an innovative Gaussian Aware Temporal Scaling (GATS) framework for robust spatio-temporal modeling of 4D point cloud videos, which effectively

addresses distributional uncertainty and temporal scale bias through the joint design of uncertainty guided Gaussian convolution and temporal scaling attention. Distinctively, we are the first to analyze point cloud dynamics from the perspective of relative velocity, providing a principled solution to frame rate inconsistency and motion representation stability. Extensive experiments demonstrate that GATS consistently enhances performance across multiple benchmarks, highlighting both its theoretical significance and practical value for real world 4D point cloud understanding.

References

- [1] Yizhak Ben-Shabat, Oren Shrouf, and Stephen Gould. 3d-naction: Understanding human actions in 3d point clouds. In *Proceedings of the IEEE/CVF Conference on Computer Vision and Pattern Recognition*, pages 19978–19987, 2024. 6
- [2] Carlos Caetano, Jessica Sena, François Brémond, Jefferson A Dos Santos, and William Robson Schwartz. Skelemotion: A new representation of skeleton joint sequences based on motion information for 3d action recognition. In *2019 16th IEEE international conference on advanced video and signal based surveillance (AVSS)*, pages 1–8. IEEE, 2019. 6
- [3] Christopher Choy, JunYoung Gwak, and Silvio Savarese. 4d spatio-temporal convnets: Minkowski convolutional neural networks. In *Proceedings of the IEEE/CVF conference on computer vision and pattern recognition*, pages 3075–3084, 2019. 6
- [4] Hehe Fan and Yi Yang. Pointrrnn: Point recurrent neural network for moving point cloud processing. *arXiv preprint arXiv:1910.08287*, 2019. 1, 2, 3
- [5] Hehe Fan, Yi Yang, and Mohan Kankanhalli. Point 4d transformer networks for spatio-temporal modeling in point cloud videos. In *Proceedings of the IEEE/CVF conference on computer vision and pattern recognition*, pages 14204–14213, 2021. 1, 2, 3, 6
- [6] Hehe Fan, Xin Yu, Yuhang Ding, Yi Yang, and Mohan Kankanhalli. Pstnet: Point spatio-temporal convolution on point cloud sequences. In *International Conference on Learning Representations*, 2021. 2, 6
- [7] Hehe Fan, Xin Yu, Yi Yang, and Mohan Kankanhalli. Deep hierarchical representation of point cloud videos via spatio-temporal decomposition. *IEEE Transactions on Pattern Analysis and Machine Intelligence*, 44(12):9918–9930, 2021. 6
- [8] Hehe Fan, Yi Yang, and Mohan Kankanhalli. Point spatio-temporal transformer networks for point cloud video modeling. *IEEE Transactions on Pattern Analysis and Machine Intelligence*, 45(2):2181–2192, 2022. 3, 6
- [9] Albert Gu, Tri Dao, Stefano Ermon, Atri Rudra, and Christopher Ré. Hippo: Recurrent memory with optimal polynomial projections. *Advances in neural information processing systems*, 33:1474–1487, 2020. 1
- [10] Albert Gu, Karan Goel, and Christopher Ré. Efficiently modeling long sequences with structured state spaces. In *The International Conference on Learning Representations (ICLR)*, 2022. 1
- [11] Haiyun Guo, Jinqiao Wang, Yue Gao, Jianqiang Li, and Hanqing Lu. Multi-view 3d object retrieval with deep embedding network. *IEEE Transactions on Image Processing*, 25(12):5526–5537, 2016. 1
- [12] Xiaoshui Huang, Sheng Li, Yifan Zuo, Yuming Fang, Jian Zhang, and Xiaowei Zhao. Unsupervised point cloud registration by learning unified gaussian mixture models. *IEEE Robotics and Automation Letters*, 7(3):7028–7035, 2022. 3
- [13] Linglin Jing, Ying Xue, Xu Yan, Chaoda Zheng, Dong Wang, Ruimao Zhang, Zhigang Wang, Hui Fang, Bin Zhao, and Zhen Li. X4d-sceneformer: Enhanced scene understanding on 4d point cloud videos through cross-modal knowledge transfer. In *Proceedings of the AAAI Conference on Artificial Intelligence*, pages 2670–2678, 2024. 3
- [14] Junnan Li, Yongkang Wong, Qi Zhao, and Mohan S Kankanhalli. Unsupervised learning of view-invariant action representations. *Advances in neural information processing systems*, 31, 2018. 6
- [15] Maosen Li, Siheng Chen, Xu Chen, Ya Zhang, Yanfeng Wang, and Qi Tian. Actional-structural graph convolutional networks for skeleton-based action recognition. In *Proceedings of the IEEE/CVF conference on computer vision and pattern recognition*, pages 3595–3603, 2019. 6
- [16] Wanqing Li, Zhengyou Zhang, and Zicheng Liu. Action recognition based on a bag of 3d points. In *2010 IEEE computer society conference on computer vision and pattern recognition-workshops*, pages 9–14. IEEE, 2010. 6
- [17] Xing Li, Qian Huang, Zhijian Wang, Tianjin Yang, Zhenjie Hou, and Zhuang Miao. Real-time 3-d human action recognition based on hyperpoint sequence. *IEEE Transactions on Industrial Informatics*, 19(8):8933–8942, 2022. 6
- [18] Dingkan Liang, Xin Zhou, Xinyu Wang, Xingkui Zhu, Wei Xu, Zhikang Zou, Xiaoqing Ye, and Xiang Bai. Pointmamba: A simple state space model for point cloud analysis. *arXiv preprint arXiv:2402.10739*, 2024. 2, 3
- [19] Jun Liu, Gang Wang, Ling-Yu Duan, Kamila Abdiyeva, and Alex C Kot. Skeleton-based human action recognition with global context-aware attention lstm networks. *IEEE Transactions on Image Processing*, 27(4):1586–1599, 2017. 6
- [20] Jun Liu, Gang Wang, Ping Hu, Ling-Yu Duan, and Alex C Kot. Global context-aware attention lstm networks for 3d action recognition. In *Proceedings of the IEEE conference on computer vision and pattern recognition*, pages 1647–1656, 2017. 6
- [21] Jiuming Liu, Guangming Wang, Weicai Ye, Chaokang Jiang, Jinru Han, Zhe Liu, Guofeng Zhang, Dalong Du, and Hesheng Wang. Diffflow3d: Toward robust uncertainty-aware scene flow estimation with iterative diffusion-based refinement. In *Proceedings of the IEEE/CVF Conference on Computer Vision and Pattern Recognition*, pages 15109–15119, 2024. 1
- [22] Jiuming Liu, Jinru Han, Lihao Liu, Angelica I Aviles-Rivero, Chaokang Jiang, Zhe Liu, and Hesheng Wang. Mamba4d: Efficient 4d point cloud video understanding with disentangled spatial-temporal state space models. In *Proceedings of*

- the Computer Vision and Pattern Recognition Conference*, pages 17626–17636, 2025. 3, 6
- [23] Lihao Liu, Angelica I Aviles-Rivero, and Carola-Bibiane Schönlieb. Contrastive registration for unsupervised medical image segmentation. *IEEE Transactions on Neural Networks and Learning Systems*, 2023. 3
- [24] Xingyu Liu, Charles R Qi, and Leonidas J Guibas. Flownet3d: Learning scene flow in 3d point clouds. In *Proceedings of the IEEE/CVF conference on computer vision and pattern recognition*, pages 529–537, 2019. 1
- [25] Xingyu Liu, Mengyuan Yan, and Jeannette Bohg. Meteor-net: Deep learning on dynamic 3d point cloud sequences. In *Proceedings of the IEEE/CVF International Conference on Computer Vision*, pages 9246–9255, 2019. 6
- [26] Yunze Liu, Junyu Chen, Zekai Zhang, Jingwei Huang, and Li Yi. Leaf: Learning frames for 4d point cloud sequence understanding. In *Proceedings of the IEEE/CVF International Conference on Computer Vision*, pages 604–613, 2023. 1
- [27] Yue Liu, Yunjie Tian, Yuzhong Zhao, Hongtian Yu, Lingxi Xie, Yaowei Wang, Qixiang Ye, and Yunfan Liu. Vmamba: Visual state space model. *arXiv preprint arXiv:2401.10166*, 2024. 1
- [28] Jun Ma, Feifei Li, and Bo Wang. U-mamba: Enhancing long-range dependency for biomedical image segmentation. *arXiv preprint arXiv:2401.04722*, 2024. 3
- [29] Eshed Ohn-Bar and Mohan Trivedi. Joint angles similarities and hog2 for action recognition. In *Proceedings of the IEEE conference on computer vision and pattern recognition workshops*, pages 465–470, 2013. 6
- [30] Omar Oreifej and Zicheng Liu. Hon4d: Histogram of oriented 4d normals for activity recognition from depth sequences. In *Proceedings of the IEEE conference on computer vision and pattern recognition*, pages 716–723, 2013. 6
- [31] Charles R Qi, Hao Su, Matthias Nießner, Angela Dai, Mengyuan Yan, and Leonidas J Guibas. Volumetric and multi-view cnns for object classification on 3d data. In *Proceedings of the IEEE conference on computer vision and pattern recognition*, pages 5648–5656, 2016. 1
- [32] Charles R Qi, Hao Su, Kaichun Mo, and Leonidas J Guibas. Pointnet: Deep learning on point sets for 3d classification and segmentation. In *Proceedings of the IEEE conference on computer vision and pattern recognition*, pages 652–660, 2017. 3
- [33] Charles Ruizhongtai Qi, Li Yi, Hao Su, and Leonidas J Guibas. Pointnet++: Deep hierarchical feature learning on point sets in a metric space. *Advances in neural information processing systems*, 30, 2017. 1, 3, 6
- [34] Guocheng Qian, Yuchen Li, Houwen Peng, Jinjie Mai, Hasan Hammoud, Mohamed Elhoseiny, and Bernard Ghanem. Pointnext: Revisiting pointnet++ with improved training and scaling strategies. *Advances in neural information processing systems*, 35:23192–23204, 2022. 1, 3
- [35] Avishkar Saha, Oscar Mendez, Chris Russell, and Richard Bowden. Translating images into maps. In *2022 International conference on robotics and automation (ICRA)*, pages 9200–9206. IEEE, 2022. 1
- [36] Amir Shahroudy, Jun Liu, Tian-Tsong Ng, and Gang Wang. Ntu rgb+d: A large scale dataset for 3d human activity analysis. In *Proceedings of the IEEE conference on computer vision and pattern recognition*, pages 1010–1019, 2016. 6
- [37] Zhiqiang Shen, Xiaoxiao Sheng, Hehe Fan, Longguang Wang, Yulan Guo, Qiong Liu, Hao Wen, and Xi Zhou. Masked spatio-temporal structure prediction for self-supervised learning on point cloud videos. In *Proceedings of the IEEE/CVF International Conference on Computer Vision*, pages 16580–16589, 2023. 3, 6
- [38] Zhiqiang Shen, Xiaoxiao Sheng, Longguang Wang, Yulan Guo, Qiong Liu, and Xi Zhou. Pointcmp: Contrastive mask prediction for self-supervised learning on point cloud videos. In *Proceedings of the IEEE/CVF Conference on Computer Vision and Pattern Recognition*, pages 1212–1222, 2023. 1, 6
- [39] Lei Shi, Yifan Zhang, Jian Cheng, and Hanqing Lu. Skeleton-based action recognition with directed graph neural networks. In *Proceedings of the IEEE/CVF conference on computer vision and pattern recognition*, pages 7912–7921, 2019. 6
- [40] Lei Shi, Yifan Zhang, Jian Cheng, and Hanqing Lu. Two-stream adaptive graph convolutional networks for skeleton-based action recognition. In *Proceedings of the IEEE/CVF conference on computer vision and pattern recognition*, pages 12026–12035, 2019. 6
- [41] Chenyang Si, Wentao Chen, Wei Wang, Liang Wang, and Tieniu Tan. An attention enhanced graph convolutional lstm network for skeleton-based action recognition. In *Proceedings of the IEEE/CVF conference on computer vision and pattern recognition*, pages 1227–1236, 2019. 6
- [42] Hang Su, Subhransu Maji, Evangelos Kalogerakis, and Erik Learned-Miller. Multi-view convolutional neural networks for 3d shape recognition. In *Proceedings of the IEEE international conference on computer vision*, pages 945–953, 2015. 1
- [43] Antonio W Vieira, Erickson R Nascimento, Gabriel L Oliveira, Zicheng Liu, and Mario FM Campos. Stop: Space-time occupancy patterns for 3d action recognition from depth map sequences. In *Iberoamerican congress on pattern recognition*, pages 252–259. Springer, 2012. 6
- [44] Jiang Wang, Zicheng Liu, Ying Wu, and Junsong Yuan. Mining actionlet ensemble for action recognition with depth cameras. In *2012 IEEE conference on computer vision and pattern recognition*, pages 1290–1297. IEEE, 2012. 6
- [45] Jun Wang, Xiaolong Li, Alan Sullivan, Lynn Abbott, and Siheng Chen. Pointmotionnet: Point-wise motion learning for large-scale lidar point clouds sequences. In *Proceedings of the IEEE/CVF Conference on Computer Vision and Pattern Recognition*, pages 4419–4428, 2022. 1
- [46] Jie Wang, Tingfa Xu, Lihe Ding, Xinjie Zhang, Long Bai, and Jianan Li. Pvnnext: Rethinking network design and temporal motion for point cloud video recognition. *arXiv preprint arXiv:2504.05075*, 2025. 6
- [47] Pichao Wang, Wanqing Li, Zhimin Gao, Chang Tang, and Philip O Ogunbona. Depth pooling based large-scale 3-d action recognition with convolutional neural networks. *IEEE Transactions on Multimedia*, 20(5):1051–1061, 2018. 6

- [48] Yue Wang, Yongbin Sun, Ziwei Liu, Sanjay E Sarma, Michael M Bronstein, and Justin M Solomon. Dynamic graph cnn for learning on point clouds. *ACM Transactions on Graphics (tog)*, 38(5):1–12, 2019. 1
- [49] Yancheng Wang, Yang Xiao, Fu Xiong, Wenxiang Jiang, Zhiguo Cao, Joey Tianyi Zhou, and Junsong Yuan. 3dv: 3d dynamic voxel for action recognition in depth video. In *Proceedings of the IEEE/CVF conference on computer vision and pattern recognition*, pages 511–520, 2020. 6
- [50] Hao Wen, Yunze Liu, Jingwei Huang, Bo Duan, and Li Yi. Point primitive transformer for long-term 4d point cloud video understanding. In *European Conference on Computer Vision*, pages 19–35. Springer, 2022. 1
- [51] Louis Wiesmann, Rodrigo Marcuzzi, Cyrill Stachniss, and Jens Behley. Retriever: Point cloud retrieval in compressed 3d maps. In *2022 international conference on robotics and automation (ICRA)*, pages 10925–10932. IEEE, 2022. 1
- [52] Yang Xiao, Jun Chen, Yancheng Wang, Zhiguo Cao, Joey Tianyi Zhou, and Xiang Bai. Action recognition for depth video using multi-view dynamic images. *Information Sciences*, 480:287–304, 2019. 6
- [53] Zhaohu Xing, Tian Ye, Yijun Yang, Guang Liu, and Lei Zhu. Segmamba: Long-range sequential modeling mamba for 3d medical image segmentation. *arXiv preprint arXiv:2401.13560*, 2024. 3
- [54] Xiaodong Yang and YingLi Tian. Super normal vector for activity recognition using depth sequences. In *Proceedings of the IEEE conference on computer vision and pattern recognition*, pages 804–811, 2014. 6
- [55] Pengfei Zhang, Cuiling Lan, Junliang Xing, Wenjun Zeng, Jianru Xue, and Nanning Zheng. View adaptive neural networks for high performance skeleton-based human action recognition. *IEEE transactions on pattern analysis and machine intelligence*, 41(8):1963–1978, 2019. 6
- [56] Zhuoyang Zhang, Yuhao Dong, Yunze Liu, and Li Yi. Complete-to-partial 4d distillation for self-supervised point cloud sequence representation learning. In *Proceedings of the IEEE/CVF Conference on Computer Vision and Pattern Recognition*, pages 17661–17670, 2023. 6
- [57] Jia-Xing Zhong, Kaichen Zhou, Qingyong Hu, Bing Wang, Niki Trigoni, and Andrew Markham. No pain, big gain: classify dynamic point cloud sequences with static models by fitting feature-level space-time surfaces. In *Proceedings of the IEEE/CVF Conference on Computer Vision and Pattern Recognition*, pages 8510–8520, 2022. 1
- [58] Lianghui Zhu, Bencheng Liao, Qian Zhang, Xinlong Wang, Wenyu Liu, and Xinggang Wang. Vision mamba: Efficient visual representation learning with bidirectional state space model. *arXiv preprint arXiv:2401.09417*, 2024. 1

GATS: Gaussian Aware Temporal Scaling Transformer for Invariant 4D Spatio-Temporal Point Cloud Representation

Supplementary Material

6. Experimental Setup

6.1. Theoretical Results

We first analyze the effect of discrete sampling on velocity estimation in point cloud videos. Let $x(t) : \mathbb{R} \rightarrow \mathbb{R}^3$ denote the continuous trajectory of a point in physical time. When the trajectory is sampled at discrete intervals Δt , the observed sequence is $x^t = x(t_0 + t \cdot \Delta t)$. The corresponding discrete velocity estimator is defined as

$$\hat{v}(t) = \frac{x^{t+\Delta t} - x^t}{\Delta t}. \quad (11)$$

This estimator deviates from the true instantaneous velocity $v(t) = \frac{dx}{dt}$. By expanding $x(t + \Delta t)$ around t using Taylor series, we obtain

$$x(t + \Delta t) = x(t) + v(t)\Delta t + \frac{1}{2}a(t)(\Delta t)^2 + o((\Delta t)^2), \quad (12)$$

where $a(t)$ denotes the acceleration. Substituting this into the discrete estimator yields

$$\hat{v}(t) = v(t) + \frac{1}{2}a(t)\Delta t + o(\Delta t). \quad (13)$$

It follows that the estimation error **grows linearly** with Δt , which leads to inconsistent velocity estimation across different frame rates.

To eliminate this dependency, we introduce a temporal scaling factor $s > 0$ and define the normalized velocity estimator as

$$\hat{v}_s(t) = \frac{x^{t+\Delta t} - x^t}{s \cdot \Delta t}. \quad (14)$$

By choosing $s = \frac{\Delta t}{\Delta t_{\text{ref}}}$, where Δt_{ref} is a fixed reference interval, the estimator becomes

$$\hat{v}_s(t) = \frac{x(t + \Delta t) - x(t)}{\Delta t_{\text{ref}}}. \quad (15)$$

This normalization maps all sequences to the same reference time scale, thereby removing sampling-rate bias. Moreover, as $\Delta t \rightarrow 0$, the normalized estimator converges to the true velocity $v(t)$.

Next, we examine how the scaling factor behaves with respect to frame density. Consider a video segment of fixed physical duration T_{seg} sampled into F frames. The discrete interval is

$$\Delta t = \frac{T_{\text{seg}}}{F}. \quad (16)$$

With a fixed reference interval $\Delta t_{\text{ref}} > 0$, the scaling factor is

$$s = \frac{\Delta t}{\Delta t_{\text{ref}}} = \frac{T_{\text{seg}}}{\Delta t_{\text{ref}}} \cdot \frac{1}{F}. \quad (17)$$

This expression shows that s is inversely proportional to the frame count F . Equivalently, for a fixed segment duration, increasing the number of frames (or equivalently, the frame rate) reduces the scaling factor.

Since $\Delta t = \frac{T_{\text{seg}}}{F}$, substituting into the definition of s yields

$$s(F) = \frac{T_{\text{seg}}}{\Delta t_{\text{ref}}} \cdot \frac{1}{F} = C \cdot F^{-1}, \quad C = \frac{T_{\text{seg}}}{\Delta t_{\text{ref}}} > 0. \quad (18)$$

The function $s(F) = CF^{-1}$ is strictly decreasing for $F > 0$, with derivative

$$\frac{ds}{dF} = -CF^{-2} < 0. \quad (19)$$

Hence, as more frames are sampled within a fixed duration, the temporal scaling factor decreases accordingly.

Finally, if we express the relationship in terms of frame rate, let the frame rate be fps and the segment length be T_{seg} . Since $F = \text{fps} \cdot T_{\text{seg}}$, the scaling factor becomes

$$s = \frac{1}{\Delta t_{\text{ref}}} \cdot \frac{1}{\text{fps}}. \quad (20)$$

Thus, for a fixed reference interval, an increase in frame rate leads to a reduction of the scaling factor, whereas a decrease in frame rate results in an increase of the scaling factor. This inverse relationship ensures that the normalized velocity estimator remains invariant to frame partitioning and robust across heterogeneous video sources.

6.2. Datasets

MSR-Action3D. This widely used dataset, captured by a first generation Kinect sensor, comprises 567 depth sequences. It features 20 distinct human action categories, totaling approximately 23,000 frames with an average sequence length of 40 frames. To ensure a direct and fair comparison with prior art, we adhere to the conventional partition, assigning 270 sequences to the training set and 297 to the testing set.

NTU RGBD. As a large scale benchmark for 3D human action recognition, this dataset contains 56,880 video samples distributed across 60 fine-grained action classes. The duration of each video clip varies, ranging from 30 to 300 frames. We adopt the standard cross subject evaluation protocol, which designates 40,320 videos for training and 16,560 videos for testing.

Synthia 4D. To assess our model’s generalization performance on dense prediction, we conduct 4D semantic segmentation experiments using the Synthia 4D dataset. Derived from the original Synthia, this dataset consists of six dynamic driving scenarios. We follow the established experimental setup from previous works, using a standard frame wise split of 19,888 frames for training, 815 for validation, and 1,886 for testing.

6.3. Training Details

MSR-Action3D. We follow P4Transformer to partition the training and testing sets. For each video, we densely sample 24 frames and sample 2048 points in each frame. We train our model on a single NVIDIA A100 GPU for 50 epochs. The SGD optimizer is employed, where the initial learning rate is set as 0.01, and decays with a rate of 0.1 at the 20-th epoch and the 30-th epoch respectively.

NTU RGBD. Consistent with prior methodologies, our data processing involves 24-frame sequences with a temporal step of 2, sampling 2048 points per frame. The training was conducted over 15 epochs with a batch size of 24 on a single NVIDIA A100 GPU. An SGD optimizer was utilized, configured with an initial learning rate of 0.01 and a cosine decay schedule to ensure stable convergence and facilitate a fair comparison.

Synthia 4D. For the Synthia 4D experiments, our model was trained for a total of 150 epochs on a single NVIDIA A100 GPU, using a batch size of 8. Each input consisted of 3-frame clips, with 16,384 points per frame. The optimization was managed by an SGD optimizer with a momentum of 0.9. We implemented a learning rate schedule featuring a 10-epoch linear warmup from an initial LR of 0.01, followed by a multi-step decay (factor of 0.1) at the 50th, 80th, and 100th epochs.

7. Network Configurations

GATS Architecture. In our GATS framework, the point cloud sequence is first fed into the **Gaussian Aware Spatio-Temporal Embedding module**. In this stage, spatial neighborhoods are modeled using Gaussian weighted convolution, which leverages local mean and covariance statistics, while the temporal dimension is processed through scaled normalized convolution. This design enables the extraction of spatio-temporal feature representations that are robust to both distributional uncertainty and frame rate variations.

Subsequently, the features are passed into a **dual branch adapter (UGGC + TSA)**. The UGGC (Uncertainty Guided Gaussian Convolution) branch enhances spatial robustness by incorporating Gaussian statistics, whereas the TSA (Temporal Scaling Attention) branch introduces scaled temporal biases to ensure cross frame consistency. The out-

puts of these two branches are fused through an uncertainty aware gating mechanism, where the gating weights are determined by the condition number of the local covariance.

The fused features are then processed by the **Transformer encoder**, where each layer consists of an Attention block and a FeedForward block. The Attention block extends the standard QKV projection and multi-head attention by incorporating temporal scaling bias, thereby guaranteeing invariance to frame partitioning. The FeedForward block is composed of LayerNorm, fully connected layers, and non-linear feedforward transformations, with residual connections to maintain training stability. By stacking multiple such layers, the model produces globally consistent and robust spatio-temporal representations.

The overall GATS architecture and the detailed attention structure are illustrated in Fig. 6, where $T \in \mathbb{R}^{M \times N \times d}$ denotes the temporal tokens and $S_{GA} \in \mathbb{R}^{M \times N \times d}$ represents the Gaussian aware tokens.

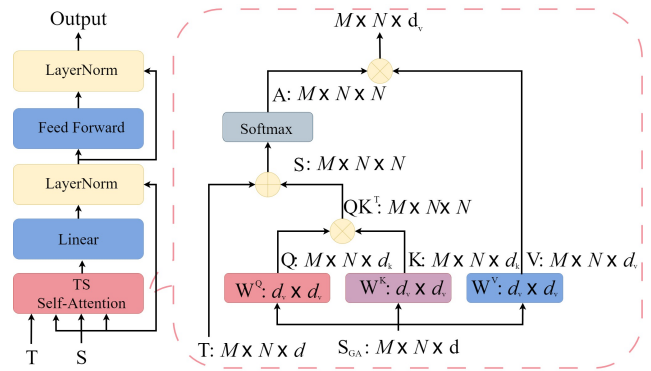


Figure 6. Structure of GATS. The left side shows the overall process, and the right side shows the specific process of DATS.

8. Additional Quantitative Results

Quantitative Results. Table 6 expands prior comparisons, showing our method achieves 97.56% accuracy, significantly outperforming depth-, skeleton-, and point-based baselines. Traditional depth-based methods such as Vieira et al. and Kläser et al. achieve 78.20% and 81.43% accuracy respectively, indicating limited capacity in capturing fine-grained motion cues. Skeleton-based approaches like Actionlet improve performance to 88.21%, benefiting from structured human pose representations. Point-based methods show mixed results: while MeteorNet reaches 88.50%, PointNet++ lags behind at 61.61%, highlighting the challenge of modeling spatio-temporal dynamics directly from raw point clouds. In contrast, our proposed GATS framework achieves a substantial improvement, reaching 97.56% accuracy. This demonstrates its superior ability to capture both spatial and temporal dependencies in 4D point cloud

sequences, validating its effectiveness for action recognition tasks.

Table 6. Action recognition accuracy comparison on a standard benchmark.

Methods	Input	Accuracy (%)
Vieira et al.	depth	78.20
Kläser et al.	depth	81.43
Actionlet	skeleton	88.21
PointNet++	point	61.61
MeteorNet	point	88.50
GATS(Ours)	point	97.56

Qualitative Results. Fig. 7 demonstrates that our model consistently delivers precise segmentation across complex scenes, underscoring its robustness and generalization. The first column displays the input frames from dynamic 4D point cloud sequences, while the second column shows the corresponding ground-truth semantic labels. The third column presents the segmentation results produced by our method. As illustrated, even in scenarios with significant spatial irregularity and temporal variation, our approach maintains high accuracy in distinguishing semantic categories. These qualitative results further validate the effectiveness of our design in handling diverse and challenging environments, highlighting its strong adaptability and generalization capability.

